Nanotechnol. Environ. Eng. (2017) 2:12
https://doi.org/10.1007/s41204-017-0024-9

ORIGINAL PAPER

Investigation of commercial $PbCrO_4/TiO_2$ for photodegradation of rhodamine B in aqueous solution by visible light

Z. M. Abou-Gamra[1] · M. A. Ahmed[1] · M. A. Hamza[1]

Received: 24 March 2017 / Accepted: 8 July 2017 / Published online: 18 July 2017

Abstract This study throws light on utilization of visible light in removal dyes from wastewater using commercial $PbCrO_4/TiO_2$(P-25) composite which was prepared by grinding TiO_2(P-25) with $PbCrO_4$ to decrease the adhesion properties of $PbCrO_4$. As-prepared catalyst was characterized by DRS, XRD and N_2 adsorption–desorption. The morphology was examined by SEM. The photodegradation of rhodamine B (Rh B) product in the presence of $PbCrO_4/TiO_2$(P-25) composite was dependent on the pH of the medium. In $2 < pH < 10$, Rh B was involved in photodegradation via *N*-deethylation terminated at rhodamine 110 while at $pH = 2$ rhodamine 110 underwent chromophore destruction. Obtained data showed that $HO_2^{\bullet}/O_2^{\bullet-}$ species were involved in degradation of dye. Commercial $PbCrO_4/TiO_2$(P-25) composite is considered as good visible light-sensitive photocatalyst for removing Rh B.

Keywords Commercial $PbCrO_4$ semiconductor · Visible light · Rhodamine B photodegradation

✉ Z. M. Abou-Gamra
zanibabougamra@yahoo.com

M. A. Ahmed
abdelhay71@hotmail.com

M. A. Hamza
chemistmahmoud13@gmail.com

[1] Chemistry Department, Faculty of Science, Ain Shams University, Cairo, Egypt

Introduction

Degradation of toxic pollutants (harmful to environment and human) is difficult. UV light is potential source for degradation of such pollutants in the presence of semiconductor. TiO_2 is a popular semiconductor due to non-toxicity, low cost, high chemical stability [1, 2]. Unfortunately, it has restricted practical applications due to its wide band gap (3.2 eV); so, it is triggered by UV radiation that represents only about 4–5% of natural solar radiation. Moreover, the mineralization processes through various redox reactions are encountered by the rapid recombination of the charge carriers. To overcome these problems, several approaches such as dye sensitization [3, 4] and composite [5, 6] are used. Recently, numerous efforts is paid to development of the visible light-driven (400–800 nm) photocatalysts (color catalysts) as visible light is abundant in solar spectrum [7, 8]. Nowadays, silver chromate (Ag_2CrO_4) is recognized as good visible light-sensitive photocatalyst due to its unique electronic and crystal structure. Ouyang et al. [9] discussed the correlation of crystal structures, electronic structures and photocatalytic properties in the three Ag-based oxides, $AgAlO_2$, $AgCrO_2$ and Ag_2CrO_4. They reported that Ag_2CrO_4 is a good photocatalyst which can remove organic contaminants under irradiation by visible light. Liu et al. [10] synthesized the Ag_2CrO_4 photocatalyst by microwave hydrothermal method. The catalyst exhibited high photocatalytic activity in degradation of pentachlorophenolate under visible light irradiation (98% after 5-h irradiation). Soofivand et al. [11] synthesized Ag_2CrO_4 and $Ag_2Cr_2O_7$ by sonochemical method using silver salicylate and silver nitrate as precursors. They reported that increasing the sonication time changes the morphology of catalyst from nanorods to nanocapsules

and nanoparticles. Photocatalytic activity of Ag_2CrO_4 was investigated by degradation of methyl orange. The percent of degradation was 87% after 280-min irradiation of visible light. Xu et al. [12] synthesized Ag_2CrO_4 by microemulsion, precipitation and hydrothermal methods to investigate the effect of preparation method on structure and photocatalytic activity of catalyst. The sample prepared by microemulsion method exhibited the highest photocatalytic efficiency on the degradation of methylene blue (MB) under visible light irradiation. Zhu et al. [13] synthesized Ag_2CrO_4 and $AgBr/Ag_2CrO_4$ by precipitation. Silver bromide enhanced the photocatalytic activity of Ag_2CrO_4 by increasing light absorption ability and enhancing the structure stability of Ag_2CrO_4. $AgBr/Ag_2CrO_4$ exhibited superior photocatalytic activity for photodegradation of rhodamine B about 93% while pure Ag_2CrO_4 degraded 73% under visible light irradiation. Luo et al. [14] synthesized Ag_2CrO_4/SnS_2 composites with different content of Ag_2CrO_4 by chemical precipitation method. The as-prepared Ag_2CrO_4/SnS_2 composites exhibited excellent photocatalytic efficiencies for the degradation of methyl orange under visible light irradiation. It was noticed that the rate constant of the Ag_2CrO_4(1.0 wt%)/SnS_2 photocatalyst is 2.2 times as high as that of pure Ag_2CrO_4 and 1.5 times larger than that of pure SnS_2, respectively. Habibi-Yangjeh and Akhundi [15] synthesized magnetic g-$C_3N_4/Fe_3O_4/Ag_2CrO_4$ nanocomposites, as visible light-driven photocatalyst, using refluxing method. As-prepared g-$C_3N_4/Fe_3O_4/Ag_2CrO_4$(20%) nanocomposite exhibited superior activity for degradation of rhodamine B under visible light irradiation. Photocatalytic activity of this nanocomposite was about 6.3- and fivefold higher than those of the g-C_3N_4 and g-C_3N_4/Fe_3O_4 samples, respectively. Furthermore, they investigated the influence of refluxing time, calcination temperature and scavengers of the reactive species on the degradation activity.

Unfortunately, Ag_2CrO_4 is slightly soluble in aqueous solution which decreases its structural stability and photocatalytic ability [13]. Therefore, this study focused on utilizing the properties of $PbCrO_4$ such as absorption in visible region and insolubility to use as visible light photocatalyst. The characterization of $PbCrO_4$/P-25 was investigated using developed techniques such as XRD, SEM, N_2 adsorption–desorption isotherm and UV–Vis spectrophotometer. Rh B was chosen as the model of pollutant and tungsten lamp 200 W as visible light source. The effects of $PbCrO_4$/P-25 dosage, initial concentration of Rh B and initial solution pH on degradation of the Rh B were investigated. The photocatalytic degradation mechanism was proposed, and the regeneration and reusability $PbCrO_4$/P-25 were also examined.

Experimental

Materials

Rh B and $PbCrO_4$ were purchased from Sigma-Aldrich. Degussa P-25 was obtained from Evonik Degussa India Pvt. Ltd.; it consists of 25 and 75% rutile and anatase phases of TiO_2, respectively, with a specific BET (Brunauer–Emmett–Teller) surface area of 50 m^2/g and primary particle size of 20 nm. All these chemicals were used without further purification. Properties of investigated dye are listed in Table 1. $PbCrO_4$/P-25 composite was prepared by grinding.

Stock solution is prepared by dissolving accurately weighed sample of dye in bidistilled water to give a concentration of 10^{-3} mol L^{-1}. Desirable concentrations of dye are obtained by serial dilution.

Methods

X-ray diffraction patterns were carried out by X'PERT-PRO-PANalytical (the Netherlands) X-ray diffractometer, with $CuK\alpha$ ($\lambda = 1.5406$ Å) radiation in the 2θ range from 4 to 80°. The scanning mode is continuous with step size of 0.02° and scan time of 0.5 s. The average crystallite sizes are calculated from the diffraction of peak broadening using the Debye–Scherrer equation, Eq. (1):

$$D = \frac{k}{\beta \cos \theta} \tag{1}$$

where D is the average crystallite size, β is the full width half maximum (FWHM) of the highest intensity peak (110 peak), k is a shape factor of the particles (it equals to 0.89), θ and λ are the diffraction angle and the wavelength of the X-rays, respectively.

Adsorption–desorption isotherms of purified N_2 at 77 K were determined using Nova 3200 system (USA). BET method was utilized to calculate the specific surface area from adsorption data. The Barrett–Joyner–Halenda model was used to estimate the average pore size from the desorption data.

The nanostructure of a prepared sample was investigated by scanning electron microscope, SEM using JEOL, model Jed 2300 (Japan) microscope.

The band gap energy of $PbCrO_4/TiO_2$ sample was determined using DRS. The band energy is calculated by Eq. (2):

$$E_g = h\frac{C}{\lambda} = \frac{1240}{\lambda} \tag{2}$$

where E_g is the band gap energy (eV), h is the Planck's constant, c is the light velocity (nm s^{-1}) and λ is the wavelength (nm).

Table 1 Properties of the investigated dye

Characteristic	Rhodamine B
Molecular structure	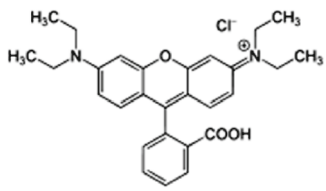
Chemical formula	$C_{28}H_{31}ClN_2O_3$
Molecular weight	479.02

pH of solution was conducted with a Griffin pH meter fitted with glass calomel electrode.

Determination of point zero charge

pH at the point of zero charge (pHpzc) for $PbCrO_4$/P-25 catalyst was determined by the batch equilibration technique [16]. Sodium chloride solution (0.1 mol/L NaCl) was used as an inert electrolyte. Initial pH values ($pH_{initial}$) of the NaCl solutions were adjusted from 2 to 12 by addition of 0.1 mol/L HCl or NaOH. 0.1 g of $PbCrO_4/TiO_2$ was added into 25 mL of 0.1 mol/L NaCl solution. The suspension mixture was allowed to equilibrate for 3 h in a shaker maintained at room temperature. Then, the suspension solution was filtered and the pH values (pH_{final}) were measured.

Photocatalytic experiments

Photocatalytic activity was evaluated by monitoring the degradation of Rh B under visible light irradiation (200 W Tungsten lamp). 100 mL aqueous solution of dye with certain amount of photocatalyst was taken in Pyrex vessel which was surrounded by a circulating water jacket to cool the sample. Prior to light irradiation, the suspension was stirred in the dark for 30 min to reach the equilibrium between the dye and catalyst. During the course of light irradiation, 5 mL aliquot was withdrawn at a various time intervals. Then the samples were centrifuged for 10 min at 1800 rpm. Supernatant concentration was determined spectrophotometrically at $\lambda_{max} = 554$ nm of Rh B using thermostat Evolution 300 UV–Vis spectrophotometer. The removal % is calculated by Eq. (3):

$$\text{Removal } \% = [(A_o - A_t)/A_o] \times 100 \quad (3)$$

where A_o and A_t are the absorbance of dye after equilibrium in dark and at time 't' of irradiation, respectively, at $\lambda_{max} = 554$ nm.

Determination of chemical oxygen

COD is the measurement of amount of oxygen in aqueous solution consumed in oxidation of pollutant in wastewater and is used to calculate the mineralization percent by Eq. (4):

$$\text{mineralization } \% = \frac{COD_b - COD_a}{COD_b} \times 100 \quad (4)$$

where COD_b and COD_a are the COD values of pure dye before and after irradiation in the presence of catalyst, respectively.

Results and discussion

Characterization of catalyst

XRD

XRD is widely used technique in the investigation of the crystalline parameters and size of the nanoparticles. Figure 1 displays the diffraction patterns of pure TiO_2 (P-25), pure $PbCrO_4$ and $PbCrO_4$/P-25 nanoparticles. On careful examination of the diffraction patterns, one can notice the interference of peak at $2\theta = 25.3$ of P-25 with that one for chromate and disappearance of 38.5 assigned to P-25 in diffractogram of $PbCrO_4$/P-25. It is interesting to notice that the crystalline pattern for the $PbCrO_4$/P-25 sample resembles the XRD pattern of the pure $PbCrO_4$. There is no remarkable change noticed for $PbCrO_4$ sample; however, a reduction in peak intensity of $PbCrO_4$ is observed. This is due to mixing of P-25 with chromate nanoparticles which reduced the concentration of chromate in $PbCrO_4$/P-25; consequently, peak intensity decreased. The analysis of our experimental results pointed out that the crystallite size of pure TiO_2(P-25), $PbCrO_4$ and $PbCrO_4$/P-25 is about 23, 77 and 72 nm, respectively, which is consistent with reported early [17].

SEM

The SEM images of pure $PbCrO_4$, TiO_2(P-25) and $PbCrO_4$/P-25 composite are shown in Fig. 2. As shown in Fig. 2, morphology of pure $PbCrO_4$ is composed of regular rods and the surface of $PbCrO_4$ is very smooth. As indicated in Fig. 2, TiO_2 (P-25) nanoparticles are distributed on the

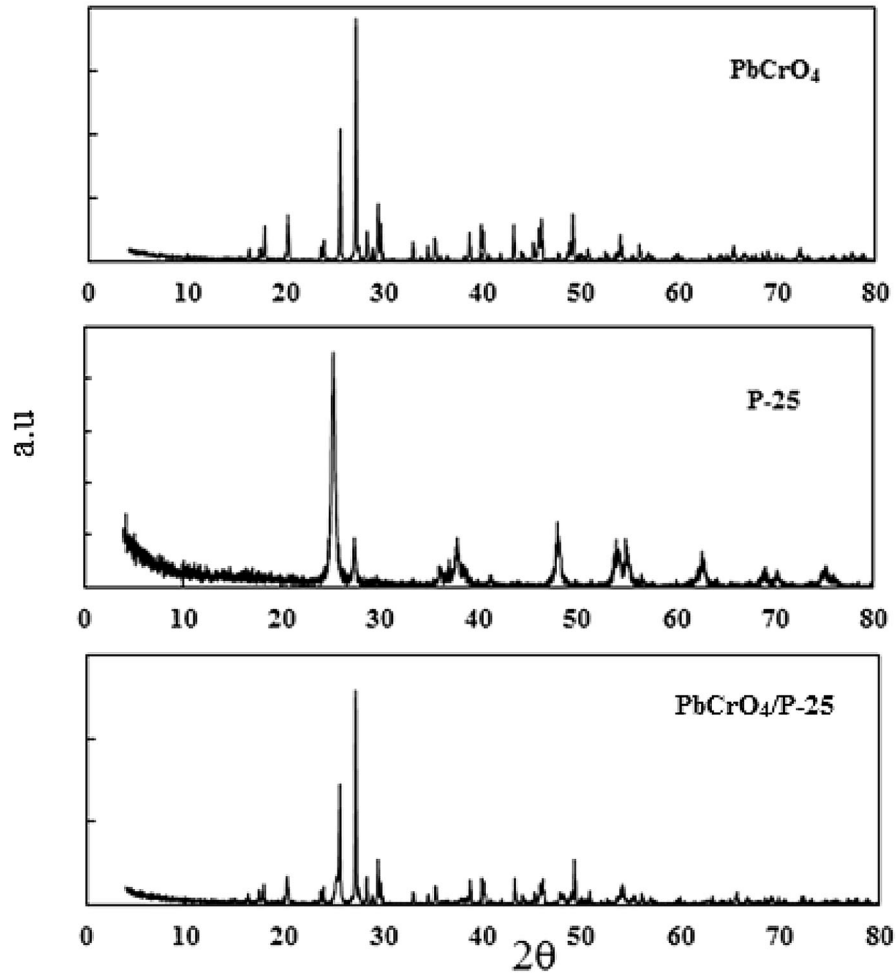

Fig. 1 XRD patterns of pure $PbCrO_4$, TiO_2 (p-25) and $PbCrO_4/TiO_2$ (p-25) composite

surface of $PbCrO_4$. The morphology of the $PbCrO_4$/P-25 composite is approximately similar to that of $PbCrO_4$ except for the relatively rough surface in the composite due to deposition of TiO_2(P-25) nanoparticles on $PbCrO_4$ surface.

DRS

The UV–Vis diffuse reflectance spectra of pure $PbCrO_4$, P-25 and $PbCrO_4$/P-25 samples are presented in Fig. 3. Pure $PbCrO_4$ shows a sharp absorption edge near 565 nm, corresponding to the band gap of 2.2 eV. Mixing P-25 with $PbCrO_4$ has no effect on absorption edge of $PbCrO_4$.

Textural characterization $PbCrO_4$/P-25 of nanoparticles

Adsorption–desorption isotherms of N_2 adsorption at 77 K on $PbCrO_4$/P-25 nanoparticles are presented in Fig. 4a. The adsorption isotherm is classified as type II according to IUPAC, exhibiting H3 hysteresis loop which refers to plate-like pores. The specific surface area (A_{BET}) of the prepared sample is about 29.43 m^2/g which was estimated by using the BET equation in its normal range of applicability and adopting a value of 16.2 Å for the cross-sectional area of N_2. However, the total pore volume (Vp) was taken at a saturation pressure and expressed as liquid volume = 0.066 cc/g. According to pore size distribution (Fig. 4b), some of pores radii are micropores with peak maximum located at 13.52 Å and other with pore radii greater than 50 Å (mesopores). t-plot (Fig. 4c) showed the presence of mixture of micropores (downward deviation) and mesopores (upward deviation) that confirmed the suggested data from pore size distribution.

Point zero charge

Figure 5 shows the plot of $pH_{initial}$ against pH_{final} of $PbCrO_4$/P-25 catalyst suspension in 0.1 M NaCl. The presence of the plateau indicates that the catalyst has amphoteric properties and acts as a buffer in this range of pH (4–8). In this range, the pH_{final} is almost the same for all values of $pH_{initial}$ and corresponds to pHpzc. The pHpzc of $PbCrO_4$/P-25 catalyst is observed to be pH 3.

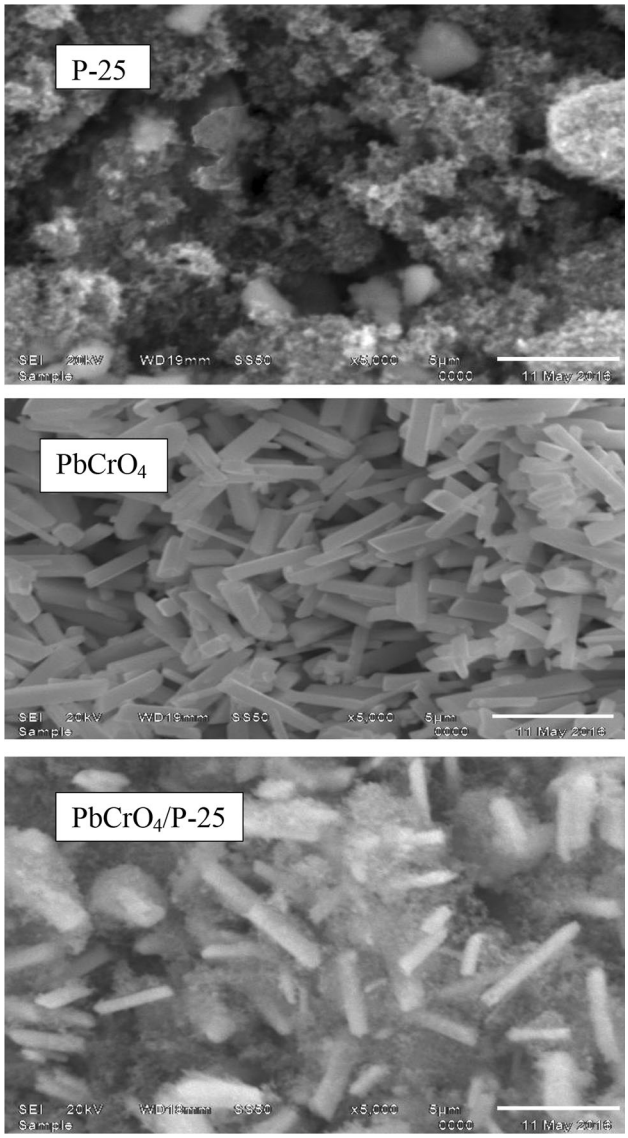

Fig. 2 SEM Images of TiO_2 (p-25), $PbCrO_4$ and $PbCrO_4/TiO_2$ (p-25) composite

Photocatalytic activity of $PbCrO_4$/P-25

Many studies focused on the evaluation of photocatalytic activity of Ag_2CrO_4 [9–12], others on the modification and improvement of their properties [13–15]. In the literature, few studies concerned with the preparation of $PbCrO_4$. Moreover, no studies concerned with photocatalytic activity of $PbCrO_4$ as visible light catalyst. Therefore, the present study concerned with photocatalytic activity of $PbCrO_4$ which evaluated by monitoring the degradation of Rh B under visible light irradiation (200 W tungsten lamp). Photocatalytic activity of $PbCrO_4$/P-25 is compared with photocatalytic activity of Ag_2CrO_4 toward different pollutants (Table 2). Table 2 shows that $PbCrO_4$/P-25 is good visible light photocatalyst in comparison with Ag_2CrO_4 which is slightly soluble in aqueous.

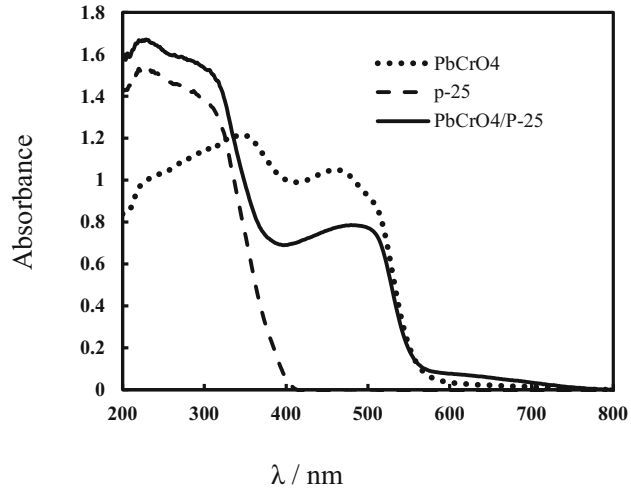

Fig. 3 DRS spectra of $PbCrO_4$, TiO_2 (p-25) and $PbCrO_4/TiO_2$(p-25) composite

The photodegradation rate was affected by several parameters such as pH, catalyst dose and initial dye concentration. Moreover, a linear plot between log A_t (absorbance of Rh B) against time was obtained, which indicates that the photocatalytic degradation of Rh B follows first-order kinetics. The rate constant for this reaction was measured by Eq. (5)

$$k = 2.303 \times \text{slope} \quad (5)$$

pH value

pH is one of the important factors controlling the adsorption of dye on adsorbent and consequently the photodegradation rate. The effect of pH studied in the range of 2–10. Increasing pH decreases the rate constant of photodegradation of Rh B (Table 3). Since PZC is about 3, the surface of catalyst is positively charged at pH values less than 3. Moreover (pK_a of COOH = 3.7 [18]), consequently expected rate at pH = 2 is the slowest one due to the repulsion between cationic Rh B and the surface of catalyst. This is contradicted with experimental results where complete photodegradation of Rh B was observed at pH = 2 (Fig. 6a); this will be discussed later.

Furthermore, at $3 < pH < 10$, drastic decrease in photodegradation rate constant was observed (Table 3). This is due to (1) repulsion between carboxylic group and negatively charged surface of catalyst and (2) aggregation of dimer resulted from electrostatic attraction between COO^- and N^+ of xanthane group of zwitterion [19, 20] which obscures reaching light to the catalyst surface. The

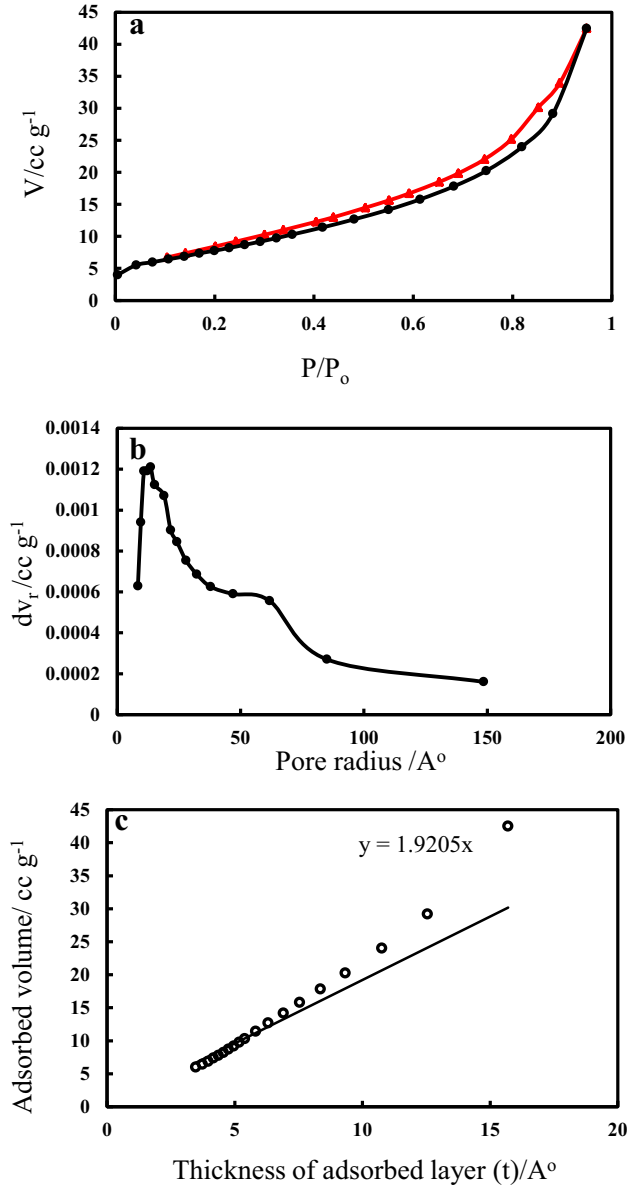

Fig. 4 N_2 adsorption–desorption isotherms (**a**), pore size distribution curve (**b**) and t-plot (**c**) for $PbCrO_4/TiO_2$ (p-25) composite

constancy of rate constant in the range of pH 4–8, (Table 3) is in coincidence with the behavior of catalyst in this pH range (Fig. 5).

At pH10 part of $PbCrO_4$ formed soluble Na_2CrO_4 and no photodegradation of Rh B was observed (Fig. 6b). This could attribute to Na_2CrO_4 works as screen which prevents reaching of light to catalyst, consequently decreasing the production of reactive oxygen species responsible of degradation of dye. To prove this, known concentration of Na_2CrO_4 added to photocatalytic batch led to reduction of the removal percent to 20% on irradiation of 6 h.

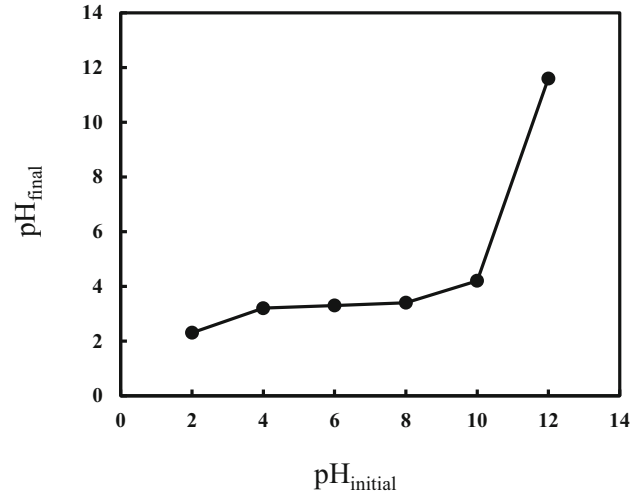

Fig. 5 Plot pH_{final} against pH $_{initial}$ for $PbCrO_4/TiO_2$ (p-25) composite in 0.1 N NaCl

Photocatalyst dose

Photocatalyst dose may affect the photodegradation of Rh B, so different amounts of photocatalyst are used. The removal percent increased from 29 to 87% by increasing the amount of photocatalyst from 0.05 to 0.5 g/100 mL. Also rate of photodegradation increased with increases in the amount of the photocatalyst (Table 3). This is attributed to the fact that as the photocatalyst amount increased, exposure surface to light increased and consequently the rate of photodegradation increased.

Rhodamine B concentration

The effect of dye concentration was studied by changing the concentration of dye in range 0.5×10^{-5}–2×10^{-5} mol dm^{-3} while other variables were kept constant. Increasing dye concentration from 0.5×10^{-5} to 2×10^{-5} mol dm^{-3} decreases the rate of degradation, from 6.17×10^{-3} min^{-1} to 1.64×10^{-3} min^{-1} (Table 3). This is attributed to dye which works as an inner filter prevents the passage of light to the semiconductor and consequently decreases the number of photoelectrons and number of photoholes, so rate of photodegradation decreases.

Radical scavenger

In order to investigate the role of reactive oxygen species ($O_2^{\bullet-}$ and $^{\bullet}OH$) involved in the photodegradation of Rh B, experiments were carried out under optimum reaction conditions (100 mL of 10^{-5} mol dm^{-3} of Rh B, 0.2 g of catalyst and irradiation time 5 h) in the presence of scavengers (10^{-5} mol dm^{-3}) such as ethanol (isopropyl alcohol) for $^{\bullet}OH$ [21], MV^{2+} for the electron [22], ascorbic

Table 2 Photocatalytic activity of $PbCrO_4$ against Ag_2CrO_4 under visible light irradiation

Catalyst and method of preparation	pollutant	Light source	Removal percent	Reference no
Ag_2CrO_4, cationic exchange of wet chemical reaction	Methyl orange	300 W Xe arc lamp	88% after 2-h irradiation	[9]
Ag_2CrO_4, microwave hydrothermal	Pentachlorophenolate	Vis light	98% after 5-h irradiation	[10]
Ag_2CrO_4, sonochemical method	Methyl orange	400 W Osram lamp	87% after 5-h irradiation	[11]
Ag_2CrO_4, microemulsion (M) precipitation (P) and hydrothermal (H)	Methylene blue	300 W Xe arc lamp	Activity of M-Ag_2CrO_4 > P-Ag_2CrO_4 > H-Ag_2CrO_4	[12]
AgBr/Ag_2CrO_4, precipitation.	Rhodamine B	5*24 W LED lamps	73 and 93% after ½ h irradiation for Ag_2CrO_4 and AgBr/Ag_2CrO_4, respectively	[13]
Ag_2CrO_4/SnS_2, chemical precipitation	Methyl orange	500 W Xe arc lamp	42.3, 54.2 and 71.1% after 2-h irradiation for Ag_2CrO_4, SnS_2 and Ag_2CrO_4/SnS_2, respectively	[14]
g-C_3N_4/Fe_3O_4/Ag_2CrO_4 (20%) nanocomposites by refluxing method	Rhodamine B	50 W LED lamp	41, 52 and 95% after 5-h irradiation for g-C_3N_4, g-C_3N_4/Fe_3O_4 g-C_3N_4/Fe_3O_4/Ag_2CrO_4 (20%), respectively	[15]
$PbCrO_4$/p-25, physical method (grinding)	Rhodamine B	200 W tungsten lamp	100% after 10 h	Present work

Table 3 Observed first-order rate constants of the photodegradation of Rh B on $PbCrO_4$/P-25 composite using 200 W tungsten lamp

[Rh B] × 10^5/M	Catalyst dose (g/100 ml)	pH	$k_o \times 10^3/min^{-1}$
1	0.2	2	18.00
		4	3.32
		6	3.03
		8	2.38
1	0.05	6	1.05
	0.10		1.77
	0.20		3.33
	0.30		4.32
	0.50		6.52
0.5	0.2	6	6.17
1			3.43
1.5			1.40
2			1.64

used as positive hole scavenger [23] and benzoquinone for $O_2^{\bullet-}$ [24]. The obtained results showed that the photodegradation percentage of Rh B was reduced from 70 to 62, 50, 50 and 48%, respectively, after the addition of MV^{2+}, isopropyl, benzoquinone and ascorbic. This is due to the decrease in the concentration of reactive oxygen species in the presence of scavengers, and therefore, both $O_2^{\bullet-}$ and $^{\bullet}OH$ were actively involved in the photodegradation process. The percentage of removal of Rh B in the presence of isopropyl and benzoquinone is almost the same. This indicates that $O_2^{\bullet-}$ and $^{\bullet}OH$ were involved in photodegradation by the same order. Furthermore, increasing the concentration of benzoquinone from 10^{-5}M to 10^{-4}M decreases the removal percent of Rh B from 50 to 30% which refers to involvement of $O_2^{\bullet-}$ in photodegradation; i.e., $O_2^{\bullet-}$ has pronounced role in photodegradation of Rh B.

The product of photocatalytic decomposition of Rh B

Figure 7 shows the temporal UV–Vis change of Rh B in the presence of $PbCrO_4$/P-25 under irradiation by visible light at natural pH. The decomposition of Rh B is accompanied by hypsochromic shift from 554 to 500 nm with color changed from rose to fluorescent yellowish green. According to earlier reports [18, 25–29], deethylation product (546, 532, 504, 500 nm) is corresponding to *N*,*N*-diethyl-*N*′-ethyl rhodamine 110, *N*-ethyl-*N*′-ethyl rhodamine 110, *N*-diethyl rhodamine 110 and rhodamine 110, respectively. This is attributed to dye anchor on the surface of catalyst via N^+ near to adsorbed O_2. Moreover, at pH = 2 complete photodegradation of rhodamine 110 was obtained as presented in Fig. 6a. This is attributed to formation of HO_2., which is more reactive than $O_2^{\bullet-}$ in acidic medium [30] and it has high redox (+1.44 V vs. NHE) in comparison with redox potential of $O_2^{\bullet-}$ (+ 0.89 V vs. NHE) [18]. It can say that under visible light irradiation, Rh B underwent two competitive processes which occurred simultaneously during the photoreaction:

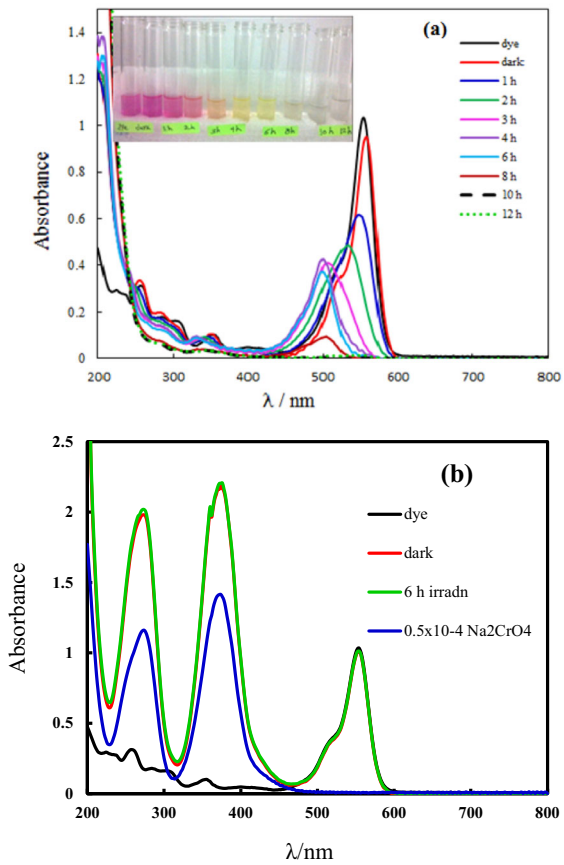

Fig. 6 UV–Vis spectra for photodegradation of Rh B on $PbCrO_4/TiO_2$ (p-25) using 200 W tungsten lamp, pH = 2 (**a**) and pH = 10 (**b**), *inset color* change of Rh B with time [Rh B] = 10^{-5} M 0.2 g/100 ml $PbCrO_4/TiO_2$ (p-25) (color figure online)

(1) *N*-deethylation processes are preceded by formation of a nitrogen-centered radical and (2) destruction of dye chromophore structure is preceded by generation of a carbon-centered radical [18, 25, 26].

Mineralization

The photocatalytic experimental results indicate a pronounced reduction in the intensities of the bands at 554 and 300 nm, suggesting that both chromophore and aromatic parts of rhodamine B were breaking down (Fig. 6a). The chemical oxygen demand (COD) is the amount of oxygen equivalent to the amount of organic and inorganic matter in the sample. A remarkable reduction in COD is evidence for the oxidation and/or decrease in carbon content in the sample, hence indicative of the extent of mineralization. It was found that COD decreased from 16 to 5.4 mg/L after exposing the sample to visible light irradiation for 10 h at pH = 2, indicating that about 70% of dye is completely removed from the solution. This result is in agreement with the photodegradation (Fig. 6a).

Mechanism

From obtained results, the proposed mechanism is that dye and catalyst absorb visible light and dye in excited state injects electron in conduction level of catalyst which in turn transfers it to O_2 adsorbed on surface forming superoxide, $O_2^{\bullet-}$. Then superoxide reacts with cationic form of Rh B to form the final product as follows:

$$\text{Rh B}/PbCrO_4 + h\upsilon \rightarrow \text{Rh B}^*/PbCrO_4 \quad (6)$$

$$\text{Rh B}^*/PbCrO_4 \rightarrow \text{Rh B}^{+\cdot}/PbCrO_4^- \quad (7)$$

$$\text{Rh B}^{+\cdot}/PbCrO_4^- + O_2 \rightarrow \text{Rh B}^{+\cdot}/PbCrO_4 + O_2^{-\cdot} \quad (8)$$

$$HO_2^{\cdot} \leftrightarrow O_2^{-\cdot} + H^+ \quad K_a = 4.69\,[18] \quad (9)$$

$$\text{Rh B}^{+\cdot}/PbCrO_4 + O_2^{-\cdot} \rightarrow N-\text{deethylate product} \quad (10)$$

$$\text{Rh B}^{+\cdot}/PbCrO_4 + HO_2^{\cdot} \rightarrow N-\text{deethylate product} \rightarrow CO_2 + H_2O. \quad (11)$$

Stability of catalyst

Successive experiments under optimum condition were done. After each experiment, the catalyst was washed by bidistilled water several times and dried in oven at 50 °C and reused in new experiment. It was found that the photocatalytic activity was diminished, and after third cycle, the catalyst lost its activity although no change in XRD (Fig. 8).

Conclusion

This research work reflects the potentiality of $PbCrO_4$/P-25 nanoparticles as an effective and preferential photocatalyst for removal of Rh B under irradiation by visible light. The structure, crystalline and morphology feature of $PbCrO_4$/P-25 nanoparticles were investigated using XRD, BET and SEM techniques. The effects of pH, photocatalyst dose and dye concentrations were investigated. Many photocatalytic experiments were performed in the presence of various scavengers to investigate the active species which is responsible for dye degradation. The experimental results have pointed out that the rate is much suppressed in the presence of isopropyl and benzoquinone solution, revealing that $^{\bullet}OH$ and $O_2^{\bullet-}$ radicals are the main active species in the photodegradation of Rh B dye. The product of photocatalytic degradation of Rh B depended on the pH of medium. In natural pH, the product was rhodamine 110, while at pH = 2, CO_2 and H_2O were the final products.

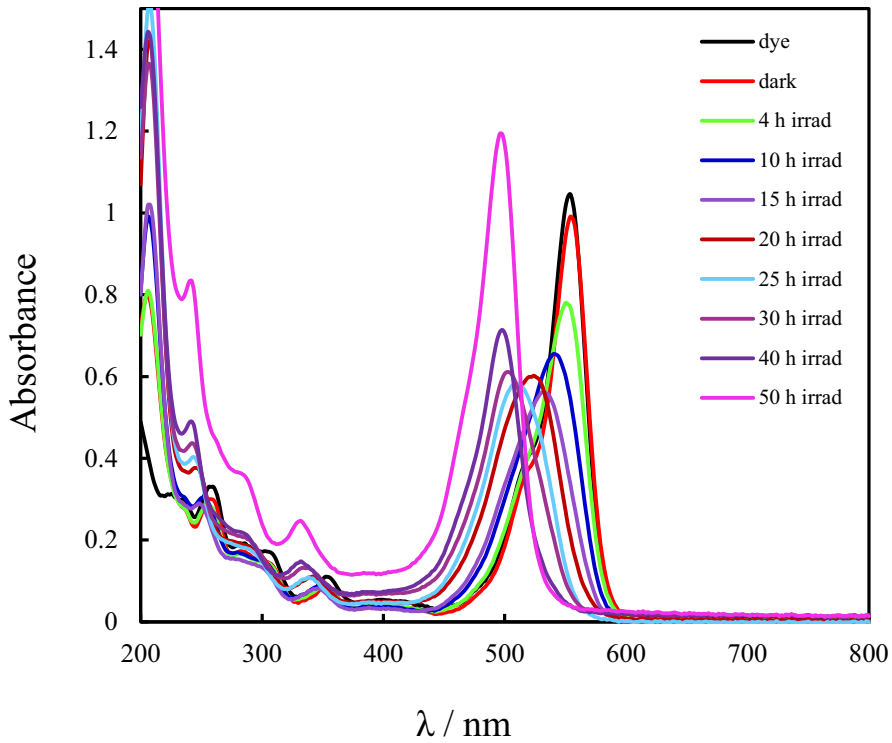

Fig. 7 UV–Vis spectra for photodegradation of Rh B on $PbCrO_4/TiO_2$ (P-25) using 200 W tungsten lamp [Rh B] = 10^{-5} M 0.2 g/100 ml $PbCrO_4/TiO_2$ (p-25) pH = 6

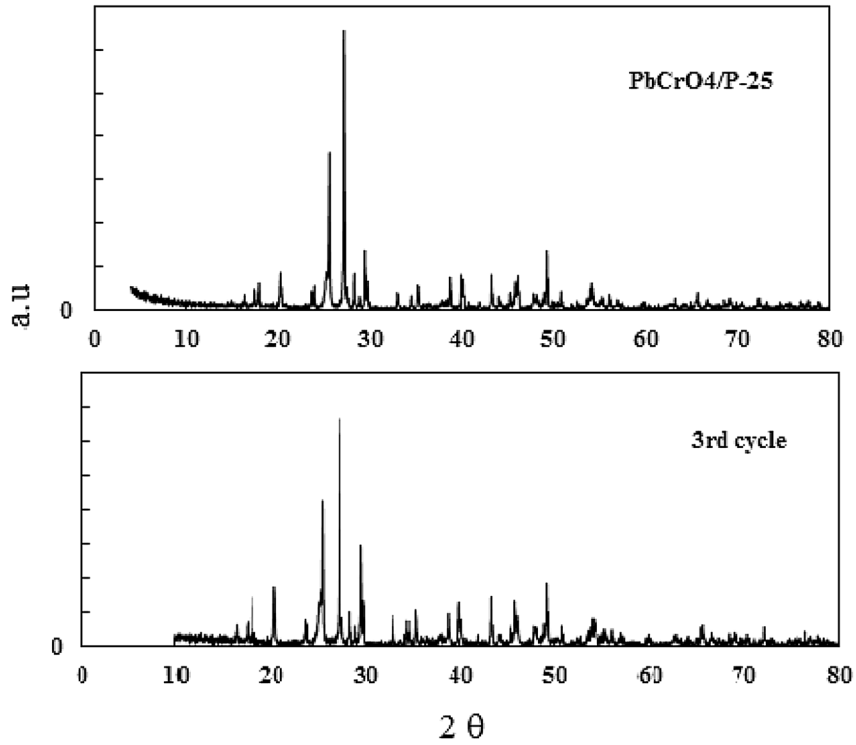

Fig. 8 XRD of photocatalyst before and after the 3rd cycle

References

1. Gupta VK, Jain R, Mittal Jain A, Saleh TA, Nayak A, Agarwal S, Sikarwar S (2012) Photo-catalytic degradation of toxic dye amaranth on TiO_2/UV in aqueous suspensions. Mater Sci Eng C 32:12–17
2. Hu A, Liang R, Zhang X, Kurdi S, Luong D, Huang H, Peng P, Marzbanrad E, Oakes KD, Zhou Y, Servos MR (2013) Enhanced photocatalytic degradation of dyes by TiO_2 nanobelts with hierarchical structures. J Photochem Photobiol A 256:7–15
3. Zhou X, Ji H, Huang X (2012) Photocatalytic degradation of methyl orange over metalloporphyrins supported on TiO_2 degussa P25. Molecules 17:1149–1158
4. Abou-Gamra ZM, Ahmed MA (2016) Synthesis of mesoporous TiO_2–curcumin nanoparticles for photocatalytic degradation of methylene blue dye. J Photochem Photobiol B 160:134–141
5. Ahmed MA, El-Katori EE, Gharni ZH (2013) Photocatalytic degradation of methylene blue dye using Fe_2O_3/TiO_2 nanoparticles prepared by sol-gel method. J Alloy Compd 553:19–29
6. Ahmed MA, Abdel-Messih MF, El-Sayed AS (2013) Photocatalytic decolorization of Rhodamine B dye using novel mesoporous SnO_2–TiO_2 nano mixed oxides prepared by sol–gel method. J Photochem Photobiol A Chem 260:1–8
7. Li T, He Y, Lin H, Cai J, Dong L, Wang X, Luo M, Zhao L, Yi X, Weng W (2013) Synthesis, characterization and photocatalytic activity of visible-light plasmonic photocatalyst AgBr–$SmVO_4$. Appl Catal B 138–139:95–103
8. Zhang L, Liang G, Wu Y, Wan Y (2015) Facile synthesis of AgBr/ZnO nanocomposite for enhanced photodegradation of methylene blue. Dig J Nanomat Biostruct 10(4):1267–1273
9. Ouyang SX, Li ZS, Ouyang Z, Yu T, Ye JH, Zou ZG (2008) Correlation of crystal structures, electronic structures, and photocatalytic properties in a series of Ag-based oxides: $AgAlO_2$, $AgCrO_2$, and Ag_2CrO_4. J Phys Chem C 112:3134–3141
10. Liu Y, Yu H, Cai M, Sun J (2012) Microwave hydrothermal synthesis of Ag_2CrO_4 photocatalyst for fast degradation of PCP-Na under visible light irradiation. Catal Commun 26:63–67
11. Soofivand F, Mohandes F, Salavati-Niasari M (2013) silver chromate and silver dichromate nanostructures: sonochemical synthesis, characterization, and photocatalytic properties. Mater Res Bull 48:2084–2094
12. Xu DF, Cao SW, Zhang JF, Cheng B, Yu JG (2014) Effects of the preparation method on the structure and the visible-light photocatalytic activity of Ag_2CrO_4. Beilstein J Nanotechnol 5:658–666
13. Zhu LF, Huang DQ, Ma JF, Wu D, Yang MR, Komarneni S (2015) Fabrication of AgBr/Ag_2CrO_4 composites for enhanced visible-light photocatalytic activity. Ceram Int 41:12509–12513
14. Luo J, Zhou X, Ma L, Xu X, Wu J, Liang H (2016) Enhanced photodegradation activity of methyl orange over Ag_2CrO_4/SnS_2 composites under visible light irradiation. Mater Res Bull 77:291–299
15. Yangjeh H, Akhundi A (2016) Novel ternary g-$C_3N_4/Fe_3O_4/Ag_2CrO_4$ nanocomposites: magneticallyseparable and visible-light-driven photocatalysts for degradation of water pollutants. J Mol Catal A Chem 415:122–130
16. Kongsri S, Janpradit K, Buapa K, Techawongstien S, Chanthai S (2013) Nano-crystalline hydroxyapatite from fish scale waste: preparation, characterization and application for selenium adsorption in aqueous solution. Chem Eng J 215–216:522–532
17. Devamani RH, Jansi Rani M (2014) Synthesis and characterization of lead chromate nanoparticles. Int Sci Res 3(4):398–402
18. Wang P, Cheng M, Zhang Z (2014) On different photodecomposition behaviors of Rhodamine B on laponite and montmorillonite clay under visible light irradiation. J Saudi Chem Soc 18:308–316
19. Abou-Gamra ZM, Medien HAA (2013) Kinetic, thermodynamic and equilibrium studies of Rhodamine B adsorption by low cost biosorbent sugar cane bagasse. Eur Chem Bull 2(7):417–422
20. Khan TA, Sharma S, Ali I (2011) Adsorption of Rhodamine B dye from aqueous solution onto acid activated mango (Magnifera indica) leaf powder: equilibrium, kinetic and thermodynamic studies. J Toxicol Environ Health Sci 3(10):286–297
21. Sohrabi MR, Ghavami M (2008) Photocatalytic degradation of direct red 23 dye usingUV/TiO_2: effect of operational parameters. J Hazard Mater 153:1235–1239
22. Singh U, Verma S, Ghosh HN, Rath MC, Priyadarsini KI, Sharma A, Pushpa KK, Sarkar SK, Mukherjee T (2010) Photo-degradation of curcumin in the presence of TiO_2 nanoparticles: fundamentals and application. J Mol Catal A Chem 318:106–111
23. Kotharia S, Vyas R, Ameta R, Punjabi PB (2005) Photoreduction of cong red by ascorbic acid and EDTA over cadmium sulphide as photocatalyst. Indian J Chem 44:2266–2269
24. Yin MC, Li ZS, Kou JH, Zou ZG (2009) Mechanism investigation of visible light-induced degradation in a heterogeneous TiO_2/Eosin Y/Rhodamine B system. Environ Sci Technol 43:8361–8366
25. Li Gu, Li X, Zhao (2000) Photooxidation pathway of Sulforhodamine-B dependence on the adsorption mode on TiO_2 exposed to visible light radiation. J Environ Sci Technol 34:3982–3990
26. Chen F, Zhao J, Hidaka H (2003) Highly selective deethylation of rhodamine B: adsorption and photooxidation pathways of the dye on the TiO_2/SiO_2composite photocatalyst. Int J Photoenergy 5:209–217
27. Wang Q, Li J, Bai Y, Lu X, Ding Y, Yin S, Huang H, Ma H, Wang F, Su B (2013) Photodegradation of textile dye Rhodamine B over a novel biopolymer–metal complex wool-Pd/CdS photocatalysts under visible light irradiation. J Photochem Photobiol B 126:47–54
28. Yu K, Yang S, He H, Sun C, Gu C, Ju Y (2009) Visible light-driven photocatalytic degradation of Rhodamine B over $NaBiO_3$: pathways and mechanism. J Phys Chem A 113:10024–10032
29. Obuya EA, Joshi PC, Gray TA, Keane TC, Jones WE (2014) Application of Pt.TiO_2 nanofibers in photosensitized degradation of Rhodamine B. Int J Chem 6(1):1–16
30. Naderhdin A, Dunford HB (1979) Oxidation of Nicotinamide adenine dinucleotide by hydroperoxyl radical, a flash photolysis study. J Phys Chem 831(5):1957–1961